Pramāṇa – J. Phys., Vol. 34, No. 1, January 1990, pp. 33–49. © Printed in India.

Positron annihilation in copper

V SUNDARARAJAN and D G KANHERE
Department of Physics, University of Poona, Pune 411 007, India

MS received 16 June 1989

Abstract. Electron momentum distribution in copper is studied through the angular correlation of positron annihilation radiation, by employing self-consistent linear combination of Gaussian orbitals band structure method. The two-photon momentum density is presented and analysed through three dimensional plots and angular momentum decomposed contributions. Calculation of two-dimensional angular correlation has been carried out in the independent particle approximation. The results for the analysis using Lock, Crisp and West theorem and the reciprocal form factors are also presented. The present theoretical results are compared with the experimental ones wherever possible, and the agreement in general, is good.

Keywords. Positron annihilation; angular correlation; copper.

PACS Nos 71·25; 78·70

1. Introduction

In recent years two experimental techniques namely, the measurement of Compton profiles (CP) and angular correlations of positron annihilation radiation (ACPAR) have emerged as powerful tools to study the ground state electronic structure of solids (Williams 1977; Brandt and Dupasquier 1983). Both the techniques probe electronic structure in momentum space and yield complementary information about electron momentum density (EMD). While CP which is related directly to EMD, serves as a useful technique to investigate the nature of the electron wavefunctions (Cooper 1985), the ACPAR measurements, especially with modern high resolution 2-dimensional (2D) machines (Berko and Mader 1975; West *et al* 1981 and Manuel 1983), yield a rich data about Fermi surface (FS) topology and are sensitive to conduction electron states as seen by positron (Berko 1983). Thus a careful comparison of theoretical calculations and the experimental data for both the techniques can provide much insight into the nature of electron states, electron-electron correlations, electron-positron correlations as well as about FS features. This has been demonstrated by recent works on Cu (Bauer and Schneider 1983, 1984a, b, 1985 and Pattison *et al* 1982) and Ni (Rollason *et al* 1987 and Sundararajan *et al* 1988) for CP and on a number of transition metals for ACPAR (Singh and Singru 1982, 1983; Genoud *et al* 1988; Singh *et al* 1986 and Matsumoto and Wakoh 1988).

The transition metals have attracted considerable interest due to the localized nature of the *d*-electrons, high degree of *sp-d* hybridization and complicated FS topology (Mijnarends 1983). The density functional (DF) theory with its impressive achievements in explaining ground state properties provides a natural and computationally tractable framework for CP and ACPAR calculations. Let us recall

that EMD is related, via Fourier transform, to the full two-particle density matrix, while the DF guarantees its diagonal elements only i.e., the charge density. Indeed the work of Bauer and Schneider (1984a, 1985) on Cu and that of Rollason *et al* (1987) on Ni have demonstrated that a careful comparison between high accuracy experimental CP and DF calculations reveals the inadequacy of the local density approximation (LDA).

The sensitivity of these experimental techniques, especially the positron annihilation technique, makes it mandatory to employ an accurate band structure method for theoretical calculations and over the years a number of band structure methods like APW (Loucks 1966), KKR (Kaiser *et al* 1986), LMTO (Singh and Jarlborg 1985) have been used. Almost all theoretical calculations for ACPAR are performed within the independent particle approximation (IPA). Such calculations missout the electron-positron correlations. To get a clear picture of EMD it is desirable to calculate the electronic structure, and related properties in momentum space, both for ACPAR and CP cases by using the same theoretical method and same electron wavefunction. The present investigation aims at calculating these properties by employing *ab initio*, all electron, self-consistent, linear combination of Gaussian orbitals (LCGO) method developed by Callaway and co-workers (Wang and Callaway 1978). We have chosen the LCGO method because of several advantages that it offers. Firstly, apart from being all electron and self-consistent, there are no shape dependent approximations e.g. Muffin-tin type. Secondly, the Gaussian nature of the basis function allows analytic evaluation of the Fourier transforms enabling us to obtain momentum density for large momentum values without loss of accuracy.

It has been realized that the comparison between experiment and theory can be fruitfully carried out by comparing not only the profiles and their anisotropies but also via Fourier transformed profiles called reciprocal form factors (Bauer and Schneider 1984a, 1985; Pattison *et al* 1982; Schulke 1977; Pattison and Williams 1976 and Singh *et al* 1985). It has a number of advantages: (1) This function emphasizes the band nature of the electrons because, the core contribution becomes negligible after about 3 a.u. (2) Any deviation between the theoretical and experimental value at $z = R$, the lattice translation vector, reflects upon the differences between the occupancy functions for the interacting and non-interacting electrons. (3) These functions are related to the off-diagonal elements of the two-particle density matrix and hence, should offer a test for density functional theory. (4) Lastly, for a metal like copper, comparison of the zero crossings of the B functions with that of the free electron case would indicate the influence of the anisotropic FS and d-wavefunctions and deviation from free electron-like behaviour.

In ACPAR the folding procedure introduced by Lock, Crisp and West (Lock *et al* 1973 and Lock and West 1975) and its extension to 2D ACPAR (Berko 1979) are turning out to be very powerful.

In the light of these developments, we have investigated the following properties: (a) TPMD, ACPAR and their anisotropies; (b) 2D ACPAR and LCW analysis; (c) Reciprocal form factors.

We have also calculated the EMD and CP using LCGO wavefunctions. The calculated profiles agree very well with CPs reported by Bagayoko *et al* (1980). Our work differs only in the lattice constant. We have used the lattice constant of 6·822 a.u. Pattison *et al* (1982) and Bauer and Schneider (1984a, b, 1985) have reported a detailed investigation of the CP for copper. Their work gave a definitive indication of

the inadequacy of the LDA and also brought out the need for an accurate theoretical calculation of EMD and CP. The recent experimental developments in CP and the status of the theory have been reviewed by Cooper (1985). In the present work the emphasis is on the application of LCGO method to positron annihilation and only the differences between EMD and TPMD are pointed out wherever appropriate.

The one-dimensional (1D) ACPAR has been reviewed by Mijnarends (1979). Cushner *et al* (1970) have reported their 1D ACPAR measurements along with their model calculation. Berko (1983) has reviewed the measurements of 2D ACPAR in copper. Recently, Matsumoto and Wakoh (1988) have compared their theoretical 2D ACPAR results with the experimental work of Haghgooie *et al* (1978) and Berko *et al* (1977). They have included electron-positron correlation effects by state dependent and character dependent enhancement factors. The present report is the first one to apply LCGO method for positron wavefunction and ACPAR calculations (Sundararajan *et al* 1988). It is hoped that this work would provide accurate profiles for meaningful quantitative comparison.

The organization of the paper is as follows. In §2 a brief outline of the LCGO formulation alongwith the relevant numerical details are given and §3 presents our results and §4 gives the summary.

2. Theory

In this section we give a brief outline of the formulation used, alongwith the definitions of the relevent quantities calculated for CP and ACPAR. The electron wavefunctions and energy bands have been calculated by self-consistent LCGO method (Wang and Callaway 1978). In this approach the Bloch functions for band index n and state $\mathbf{k}$ at position $\mathbf{r}$ are expanded as linear combination of Gaussian orbitals.

Thus,

$$\psi_n(\mathbf{k},\mathbf{r}) = \sum_i C_{ni}(\mathbf{k})\phi_i(\mathbf{k},\mathbf{r}) \tag{1}$$

where

$$\phi_i(\mathbf{k},\mathbf{r}) = (N)^{-1/2}\sum_\mu \exp(i\mathbf{k}\cdot\mathbf{R}_\mu)u_i(\mathbf{r}-\mathbf{R}), \tag{2}$$

u_i's are the individual Gaussian orbitals, $\mathbf{R}_\mu$ is the lattice vector, and N is the number of cells in the crystal volume. The expansion coefficients $C_{ni}(\mathbf{k})$ and energy eigenvalues are calculated by diagonalizing the density functional hamiltonian in the above mentioned Gaussian basis set. We have obtained self-consistency on 89 $\mathbf{k}$ points in the irreducible part of the Brillouin zone (BZ) using von Barth-Hedin exchange correlation potential as parametrized by Rajagopal *et al* (1980). The final band structure is calculated at 505 k points in the irreducible wedge of the BZ.

Positron wavefunction is also calculated under the framework of LCGO. It is written as

$$\psi_+(\mathbf{r}) = \sum_j C_j(\mathbf{k}_+ = 0)\phi_j(\mathbf{r}). \tag{3}$$

Since it gets annihilated in its ground state with $\mathbf{k}_+ = 0$ we have calculated the positron wavefunction, using the self-consistent electron potential by subtracting the exchange correlation part and changing its sign. The positron basis set consisted of 7*s*

functions. Our positron wavefunction (Sundararajan *et al* 1988) compares favourably with the previous calculation by Bross and Stohr (1974), using modified augmented plane wave method but, has a slightly higher value around 1 a.u. as compared to the wavefunction obtained by Mijnarends (1983) using symmetrized plane wave method. However, $\psi_+(r)$ calculated using the same potential under plane wave approximation is found to differ very little from the LCGO wave function.

Using electron and positron wavefunctions thus obtained, the TPMD and ACPAR can be calculated as

$$\rho^{2\gamma}(\mathbf{p}) = \sum_{n\mathbf{k}}^{\text{occ}} |F_{\mathbf{k}}^{n}(\mathbf{p})|^2 f(\mathbf{k}, n)\delta(\mathbf{k} - \mathbf{p} + \mathbf{G}), \tag{4}$$

$$N_{\hat{k}}(q) = \text{const} \times \int \mathrm{d}\mathbf{p}\rho^{2\gamma}(\mathbf{p})\delta(q - \mathbf{p}\cdot\hat{k}) \tag{5}$$

where $f(\mathbf{k}, n)$ is the Fermi-Dirac distribution function and $F_{\mathbf{k}}^{n}(\mathbf{p})$ is the electron-positron overlap integral,

$$F_{\mathbf{k}}^{n}(\mathbf{p}) = \int \exp(-i\mathbf{p}\cdot\mathbf{r})\psi_+(\mathbf{r})\psi_n(\mathbf{k}, \mathbf{r}). \tag{6}$$

The TPMD is calculated up to 4 a.u. by considering 113 **G** vectors. This generates about 42237 points in 1/48th part of the **p** space. The ACPAR values are calculated along the three symmetry directions.

It is instructive to decompose the TPMD into its *s*-, *p*- and *d*-components. Such a decomposition would provide more insight into the relative importance of the angular momentum of the electronic states. We can write the *l*-decomposed TPMD as

$$\rho_l^{2\gamma}(\mathbf{p}) = \sum_{n\mathbf{k}}^{\text{occ}} \left| \sum_{\mathbf{G}''} \sum_{i}^{n_l} \sum_{j} C_{ni}(\mathbf{k}) C_j(0) \chi_i(\mathbf{k} + \mathbf{G} - \mathbf{G}'')\chi_j(\mathbf{G}'') \right|^2 \delta(\mathbf{k} - \mathbf{p} + \mathbf{G}) \tag{7}$$

where $\mathbf{G} = \mathbf{G}' + \mathbf{G}''$. $\mathbf{G}'$ is the reciprocal lattice vector for the electron and $\mathbf{G}''$ for that of the positron. The above equation gives the pure *l*-component of TPMD wherein n_1 is the number of *l*-type orbitals used. We used 13*s*, 10*p*, 5*d* and 1*f* functions as the basis set. χ_i and χ_j are the Fourier transforms of the electron and positron basis functions respectively and written as (Rath *et al* 1973)

$$\chi_i(p) = \Omega^{-1/2} \int \exp(-i\mathbf{p}\cdot\mathbf{r}) u_i(\mathbf{r})\, \mathrm{d}\mathbf{r}. \tag{8}$$

Ω is the unit cell volume. The *l*-decomposed TPMD is calculated and presented along the ⟨100⟩, ⟨110⟩ and ⟨111⟩ directions along with the total.

We now turn to the calculations of 2D ACPAR expressed as

$$N(p_y, p_z) = \int \rho^{2\gamma}(\mathbf{p})\, \mathrm{d}p_x \tag{9}$$

where p_x is the direction of integration. The above quantity was calculated for three integration directions. The 2D ACPAR curves $N(p_y, p_z)$ thus calculated have been remapped from the *p* space to the *k* space using the LCW folding procedure governed

by the relation,

$$\tilde{N}(k_y, k_z) = \sum_{\mathbf{H}} N(p_y + H_y, p_z + H_z) \tag{10}$$

where H_y and H_z are the components of the full reciprocal lattice vectors on the (p_y, p_z) plane. The $\tilde{N}(k_y, k_z)$ distributions so obtained can be compared with the experimental results. Recently the validity of the LCW theorem for the analysis of ACPAR data has been examined by Singh and Singru (1984), Rabou and Mijnarends (1984) and Kaiser *et al* (1986, 1987). The work of Kaiser *et al* (1986) in particular, has shown that a realistic application of the LCW theorem to ACPAR data should be carried out in terms of the Bloch **k**-space density $\rho^{2\gamma}(\mathbf{k})$ which, in turn, requires a proper band structure calculation of $\rho^{2\gamma}(\mathbf{p})$.

Yet another useful way to compare theory and experiment is via Fourier transform of the momentum density i.e., $B(\mathbf{r})$ functions, which are also called the reciprocal form factors (Shulke 1977; Pattison and Williams 1976),

$$B(\mathbf{r}) = (2\pi)^{-3/2} \int \exp(-i\mathbf{p}\cdot\mathbf{r})\rho(\mathbf{p})\,\mathrm{d}\mathbf{p}. \tag{11}$$

Where $\rho(\mathbf{p})$ is the EMD. It has been shown that

$$B_{\hat{k}}(0, 0, z) = (2\pi)^{-1/2} \int \exp(-izq) J_{\hat{k}}(q)\,\mathrm{d}q \tag{12}$$

in which, $J_{\hat{k}}(q)$ is the CP along the direction $\hat{k}$. Similarly, for $N_{\hat{k}}(q)$,

$$B^{2\gamma}_{\hat{k}}(0, 0, z) = (2\pi)^{-1/2} \int \exp(izq) N_{\hat{k}}(q)\,\mathrm{d}q. \tag{13}$$

In the rest of the paper $B(0, 0, z)$ and $B^{2\gamma}(0, 0, z)$ would be denoted respectively as $B^{CP}(z)$ and $B^{2\gamma}(z)$ or as B^{CP} and $B^{2\gamma}$, depending on the context.

Equations (1) to (13) form the basis of our calculations and the results obtained are presented in the next section.

3. Results and discussion

As mentioned in the introduction, the self-consistent electron wavefunctions and the positron wavefunction calculated in IPA have been used to investigate a number of properties relevant for CP and ACPAR studies. Specifically, we present our results for TPMD, 1D ACPAR, 2D ACPAR, $B^{2\gamma}$ and $B^{2\gamma}$ functions. Since a detailed analysis of the differences between experimental and theoretical CP has been presented by Bauer and Schneider, our emphasis in this report will be on TPMD and 1D and 2D ACPAR.

3.1 *TPMD*

Conventionally, the TPMD is presented and discussed in terms of band by band contributions along three symmetry directions. Our calculations for EMD as well as TPMD depict the familiar nature along three directions showing the drops or

discontinuities at Fermi momentum with corresponding Umklapp images (Mijnarends 1973; Kanhere and Singru 1977 and Mijnarends and Singru 1979). Bross (1982) has shown the momentum density as a function of p_x in the plane $p_z=0{\cdot}05(2\pi/a)$ for different values of p_y. Such a graph gives information on the discontinuities and the anisotropic nature of the momentum density. However, to gain more insight into the nature of TPMD, it is instructive to plot its sections by symmetry planes as 3*D* perspective plots. Figures 1(a) and 1(b) show such 3*D* plots of the section of TPMD by (100) and (110) planes respectively. The corresponding zone structure is also shown with the same scale and with the same perspective view. The anisotropic nature of the momentum density is immediately clear by examination of these figures. The differences in the Umklapp contribution in these planes are also apparent. For example, in (100) the first drops in figure 1(a) clearly depict the FS structure in the first BZ. But its Umklapp images in the 2nd zone are dominant only in ⟨100⟩ direction. The effect of neck can be clearly seen in figure 1(b) i.e., in the section by (110) plane. It is interesting to note that only near ⟨111⟩ line the drops are absent including the discontinuities due to Umklapp process. Amongst all the three sections the higher zone effects are more prominent in (110) plane and least in (111) plane (not shown). A comparison of EMD plots (not shown) with TPMD plots shows that TPMD has very similar features as that of EMD. However, the first zone drops are much sharper and the Umklapp contribution is less prominent in TPMD. This is to be expected because, the different angular momentum components of the electron wavefunctions viz. *s*, *p*, *d* are spanned differently by positron.

This aspect can be brought out more clearly by making angular momentum decomposition of EMD and TPMD (eq. (7)). Such a decomposition of TPMD is shown in figures 2(a)–2(c) for the three symmetry directions. In each of these figures the total TPMD is shown by unlabelled line while *s*-, *p*- and *d*-components by labelled lines. It may be mentioned that the *s*-, *p*- and *d*-contributions will not add up to the total TPMD, since the total TPMD contains the hybridization terms also. We can somewhat quantify the relative contributions by the ratio of the weighted area under each component to the total area. Table 1 presents these ratios for both EMD and TPMD. A comparison of the *s*-, *p*- and *d*-contributions for the three directions indicates that the *d*-contribution is the least along ⟨111⟩ direction. This is reflected in the high momentum components along ⟨100⟩ and ⟨110⟩ directions. A comparison of EMD and TPMD through the figures in table 1 shows that the relative contribution from *d*-component reduced for the case of positron in all the three directions as compared to EMD. In both the cases there is a relatively high *p*-component along ⟨111⟩ direction indicating dominant *p*-character of the wavefunctions especially near the neck. It may be pointed out that the width of the *d*-band is smallest for copper and it lies well below the Fermi level, while for other 3*d* metals the Fermi level lies in the midst of the *d*-band complex (Kanhere and Singru 1977). The angular momentum decomposition analysis along the lines presented here would be fruitful for the systematic understanding of the *d*-band contribution when applied to other 3*d*-metals.

3.2 *ACPAR and LCW theorem*

The present work is the first in applying the LCGO method to positron annihilation studies. A preliminary report of the 1D ACPAR and its anisotropies has been presented elsewhere (Sundararajan *et al* 1988). Comparison of the theoretical

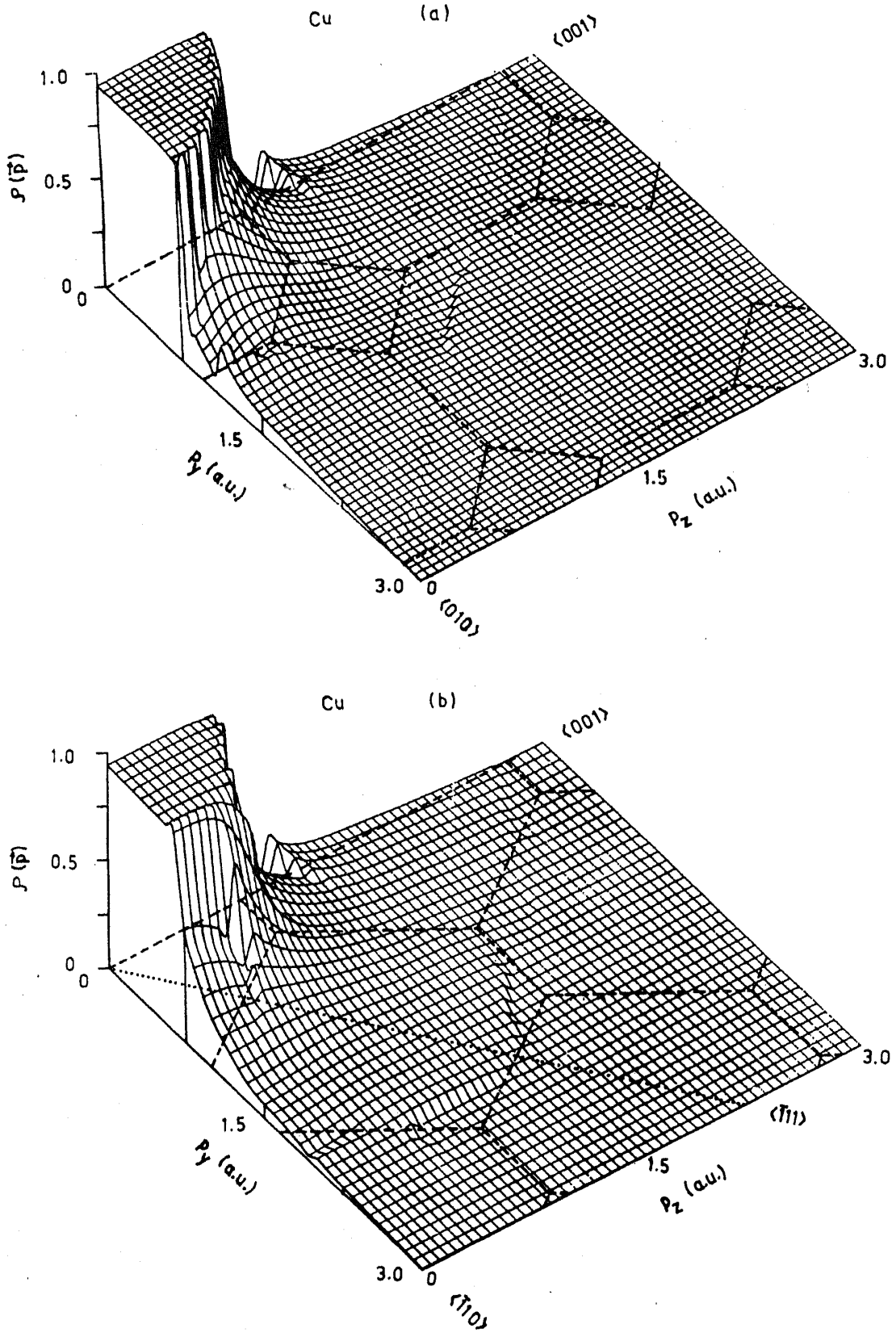

Figure 1. Sections of band TPMD for copper by the planes (**a**)(100) and (**b**)(110). The corresponding zone structure is also displayed. Dotted line in (b) shows the Λ line in the (110) plane.

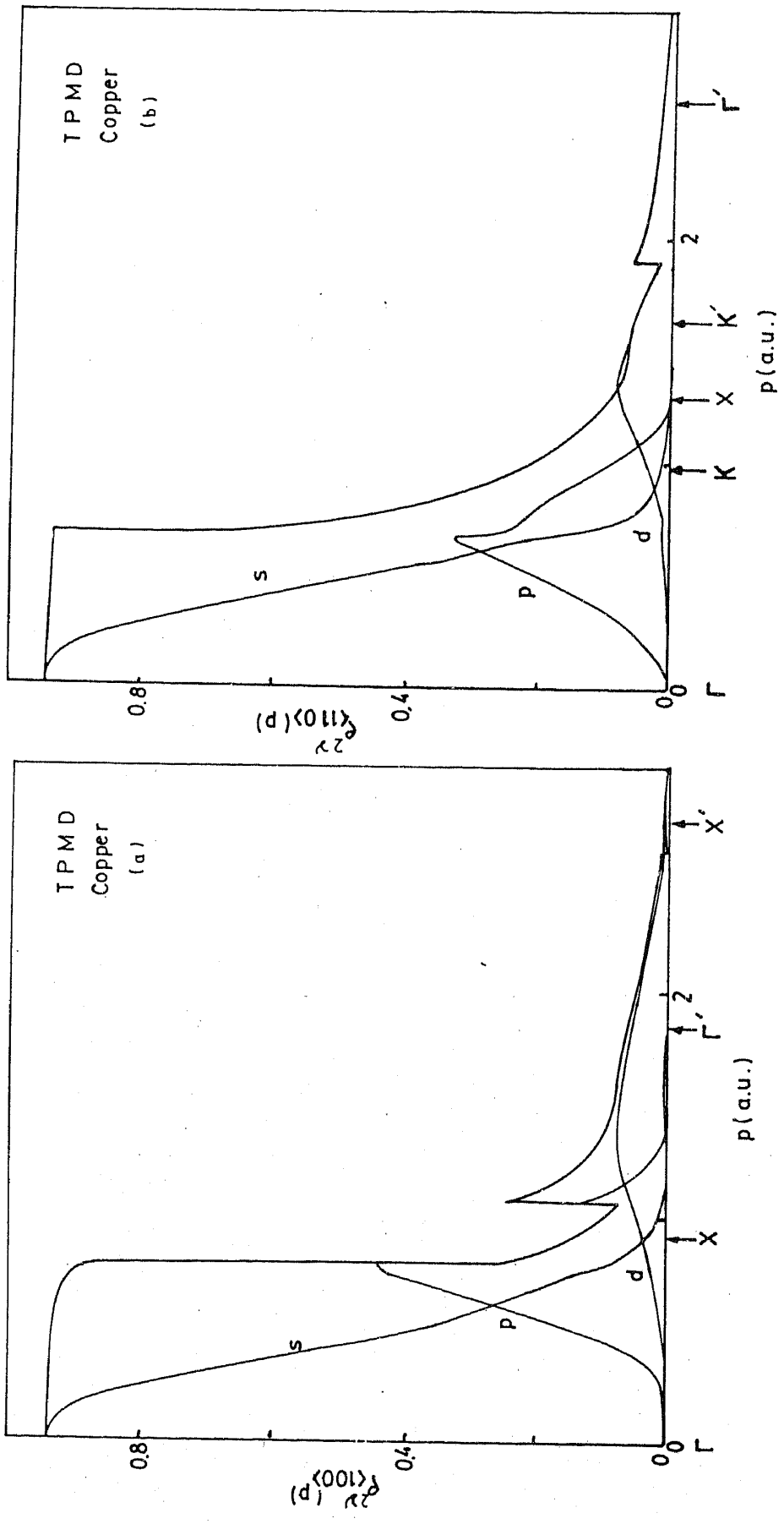
TPMD
Copper
(b)
s
p
d
Γ
K
X
K'
2
Γ'
p(a.u.)
0.0
0.4
0.8
TPMD
Copper
(a)
s
p
d
Γ
X
Γ', 2
X'
p(a.u.)
0.0
0.4
0.8

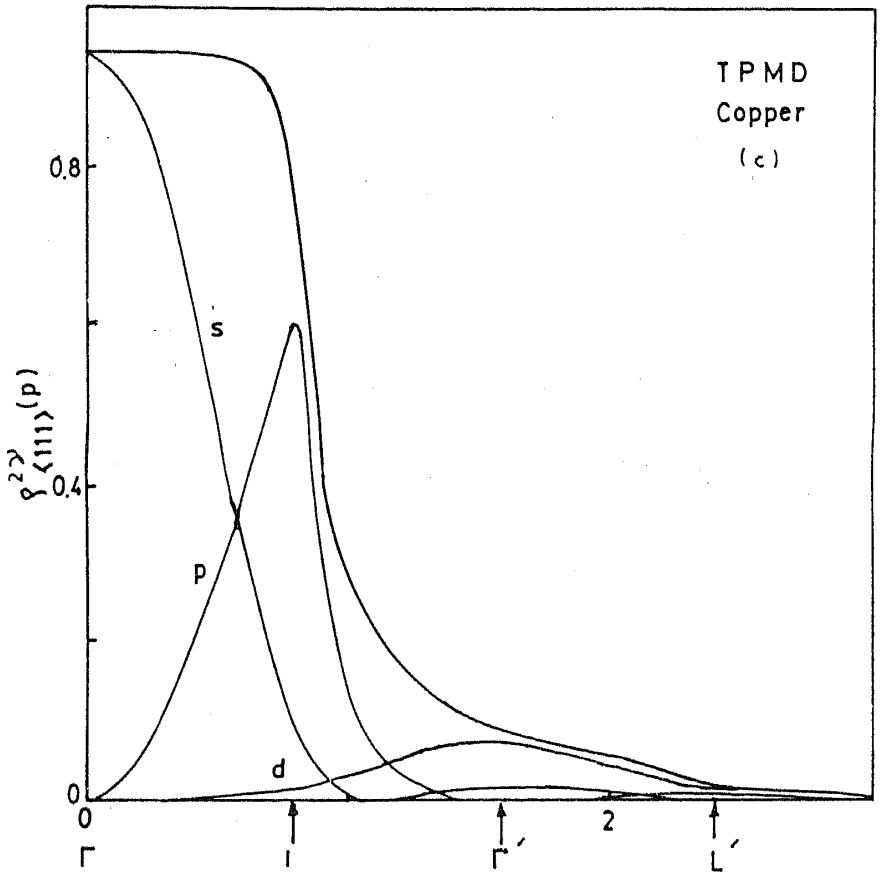

Figure 2. Band TPMD alongwith the angular momentum decompositions on three symmetry directions (**a**) ⟨100⟩, (**b**) ⟨110⟩ and (**c**) ⟨111⟩. Unlabelled line corresponds to total EMD. Individual *s*, *p*, *d* contributions are shown by labelled lines.

Table 1. Ratio of the weighted areas of pure *s*-, *p*-, *d*-contributions to the total momentum density.

Direction	*s*		*p*		*d*	
	EMD	TPMD	EMD	TPMD	EMD	TPMD
⟨100⟩	0·056	0·137	0·052	0·131	0·833	0·559
⟨110⟩	0·053	0·135	0·059	0·167	0·850	0·554
⟨111⟩	0·065	0·117	0·104	0·284	0·789	0·434

anisotropies with the experimental (Cushner *et al* 1970) ones were very good. The remaining discrepancies are attributed to the electron-positron correlation effects.

In this section we discuss the 2D ACPAR results obtained by the LCGO method for copper. The 2D ACPAR surfaces are presented in figures 3(a) and 3(b) respectively for the two integration directions viz. ⟨100⟩ and ⟨111⟩. In general the agreement with the experimental surfaces (Haghgooie *et al* 1978; Berko *et al* 1977) is good. It may be mentioned that, in an earlier calculation of 2D ACPAR using APW method by Wakoh *et al* (1979), for the case of ⟨100⟩ two small horns due to neck in the FS are prominently seen. In the present case they are less pronounced and are comparable with the experimental result. The agreement of the features in ⟨111⟩ direction with the

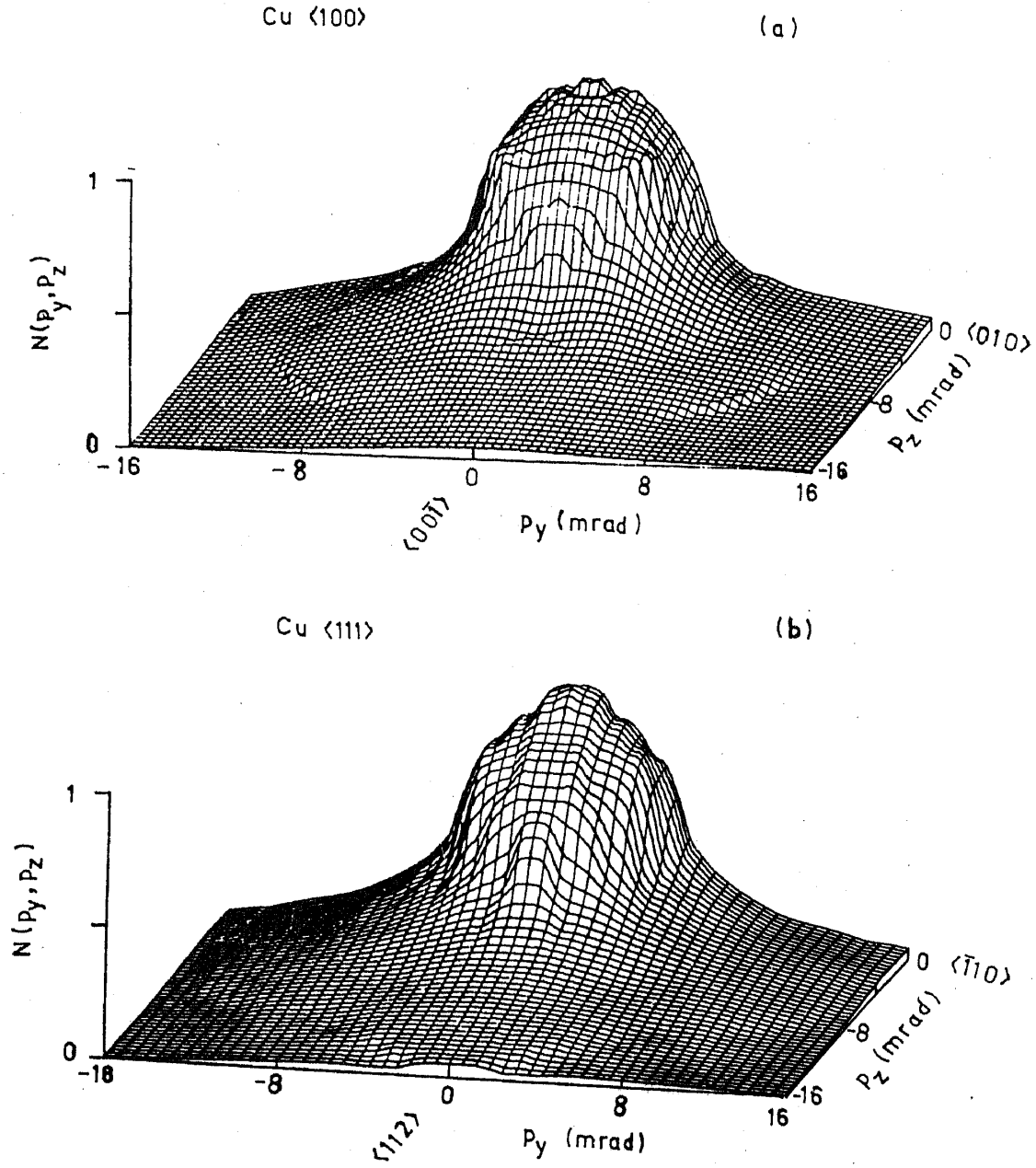

Figure 3. Theoretical band 2D ACPAR plots along the three integration directions (a) ⟨100⟩ and (b) ⟨111⟩.

experimental ones is also good, especially, the neck in the FS is clearly visible. The comparison of the results, in the three integration directions, among themselves reveal the anisotropic nature of the 2D ACPAR surface. Another observation worthy of mention here is that, theoretical surfaces show sharper structures than the experiments (Singh and Singru 1982, 1983). It is expected that the inclusion of the electron-positron enhancement effects should make these structures less sharp.

In the work of Matsumoto and Wakoh (1988), APW results have been compared with the experiment (Haghgooie *et al* 1978 and Berko *et al* 1977) through the cross-sections of 2D ACPAR surface for ⟨100⟩ and ⟨111⟩ integration directions. A similar comparison is presented in figures 4(a)–4(c). For this purpose, we added 0·2 times the

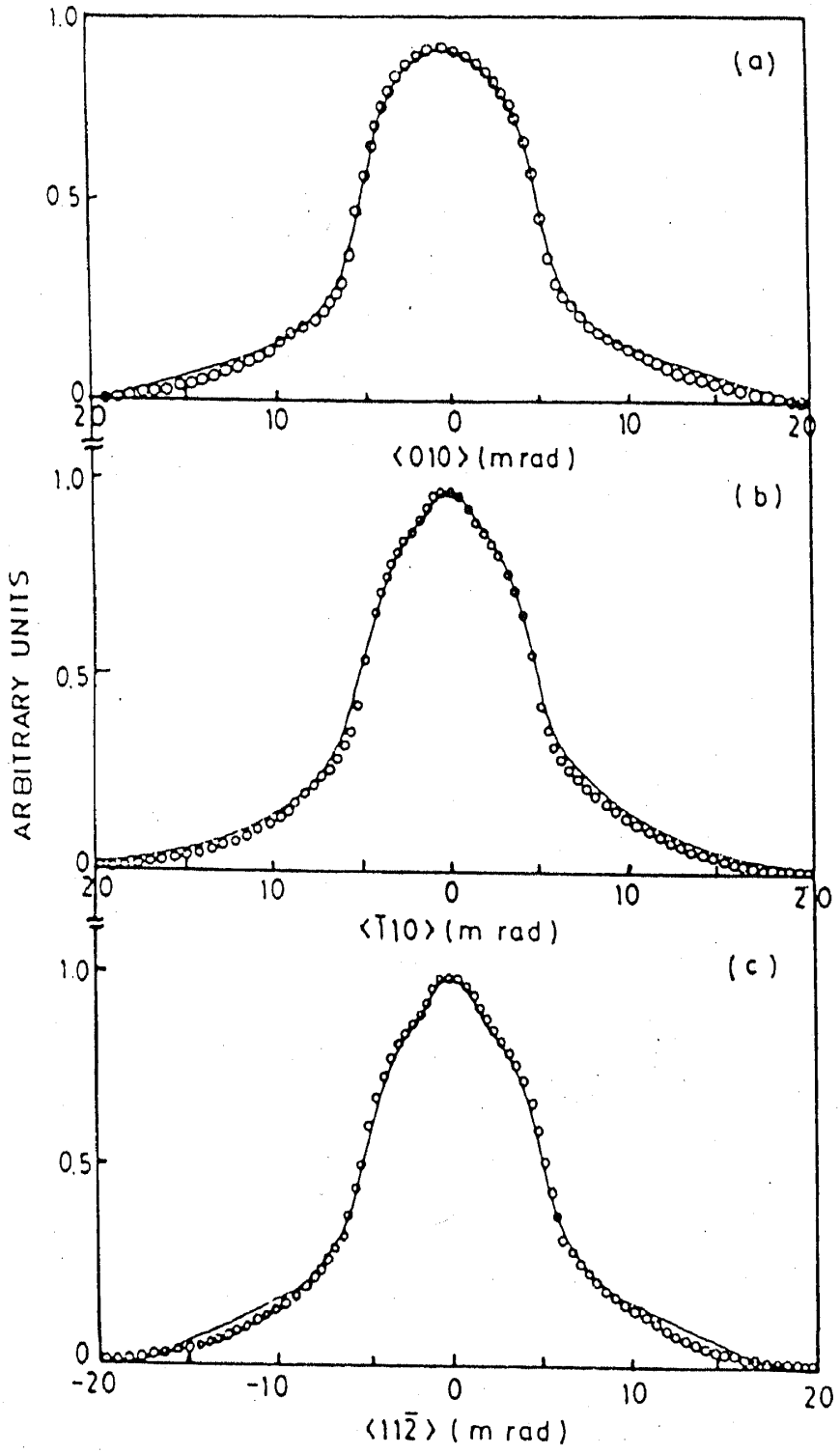

Figure 4. The cross sections of 2D ACPAR. (**a**) along the ⟨010⟩ direction and $P_{\langle 010\rangle}=0$, (**b**) along the ⟨$\bar{1}$10⟩ direction and $P_{\langle 11\bar{2}\rangle}=0$ and (**c**) along the ⟨11$\bar{2}$⟩ direction and $P_{\langle \bar{1}10\rangle}=0$. Continuous curve – theory, circles – experiment.

core contribution, as done by them, to the band result and then convoluted with the experimental resolution function. The core 2D ACPAR is calculated using the density functional wavefunctions obtained through the LCGO method. The agreement with the experiment is very good but for minor differences.

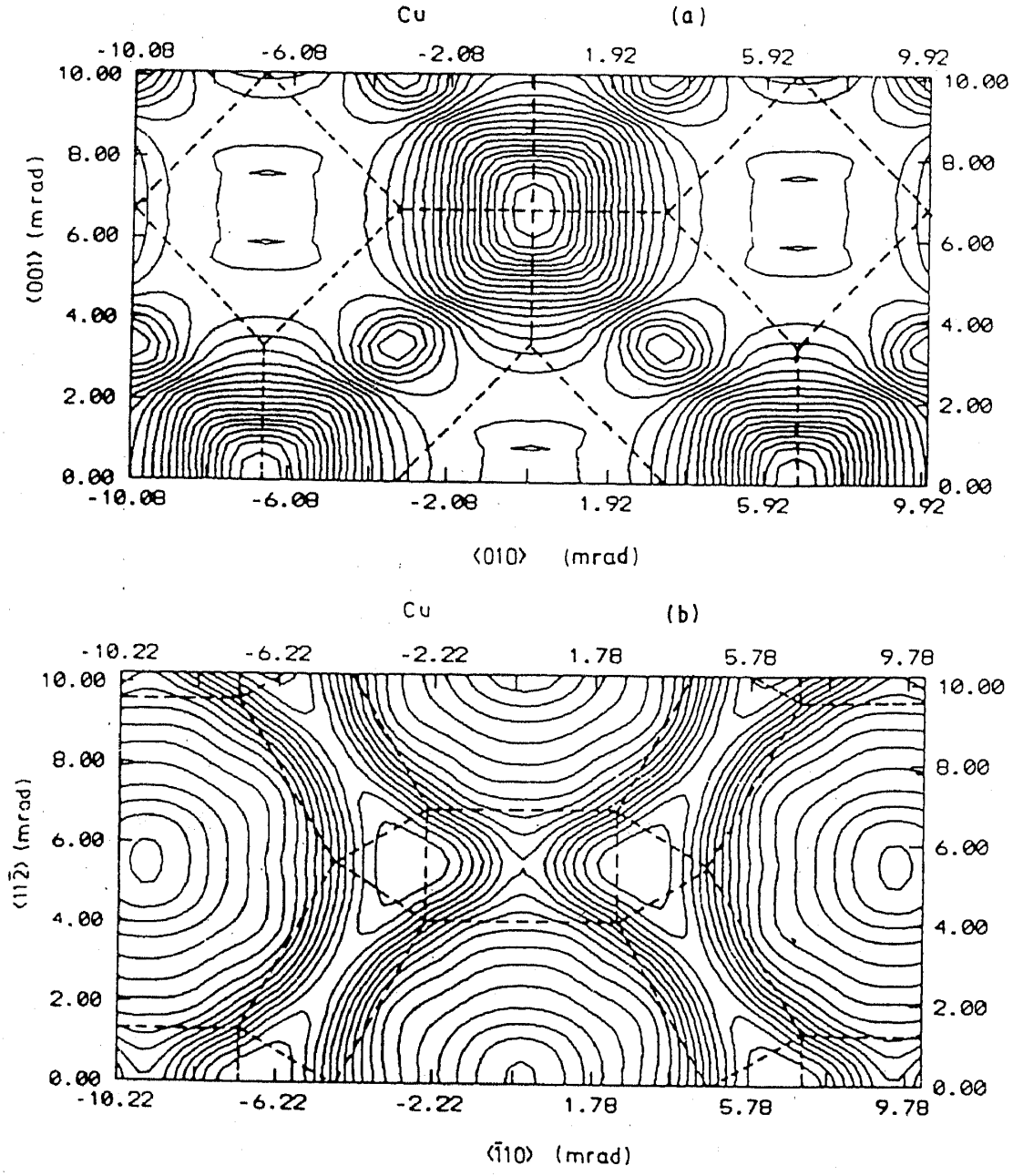

Figure 5. LCW folded 2D ACPAR contours for (**a**) (100) and (**b**) (111) planes.

We remapped the total convoluted 2D ACPAR from p space to k space using eq. (10). The resulting LCW folded densities are shown in figures 5(a) and 5(b) for the ⟨100⟩ and ⟨111⟩ integration directions respectively. These contours compare well with the experiment as well as with the APW calculation of Matsumoto and Wakoh (1988). The projection of the BZ corresponding to the (100) and (111) planes are superimposed by dotted lines which guide us to give an idea of the FS shape as reflected by LCW folded density.

It may be mentioned that the present 1D and 2D ACPAR results do not correct for the electron-positron correlation via the enhancement factors. We are unable to carry out such an analysis meaningfully because of the non-availability of the experimental

data in terms of tables. This still leaves us an option of taking into account the enhancement effects by using one of the schemes proposed by Kahana (1963), Mijnarends and Singru (1979) or Matsumoto and Wakoh (1987). However, the utility of such a procedure in the absence of experimental numerical data is somewhat limited since, only qualitative comparison is then possible. Moreover, a number of workers have reported the enhancement factor analysis on 3*d*-metals. Their work indicate that the enhancement factors are state, character or energy dependent (Matsumoto and Wakoh 1987 and Singh *et al* 1986). It is hoped that the present data would be useful to experimentalists for detailed electron-positron correlation analysis.

3.3 *Reciprocal form factors*

We present our results on $B^{CP}(z)$ and $B^{2\gamma}(z)$ along the three directions in figures 6(a)–6(c) Both the CP and ACPAR include the core contributions. The arrows indicate the lattice translation vectors and their projections on the direction under consideration. In table 2 we present the values of these vectors and the corresponding values for B functions. Our value for $B^{CP}(z)$ at $z = R_{110}$ is 0·141 as compared to the experimental

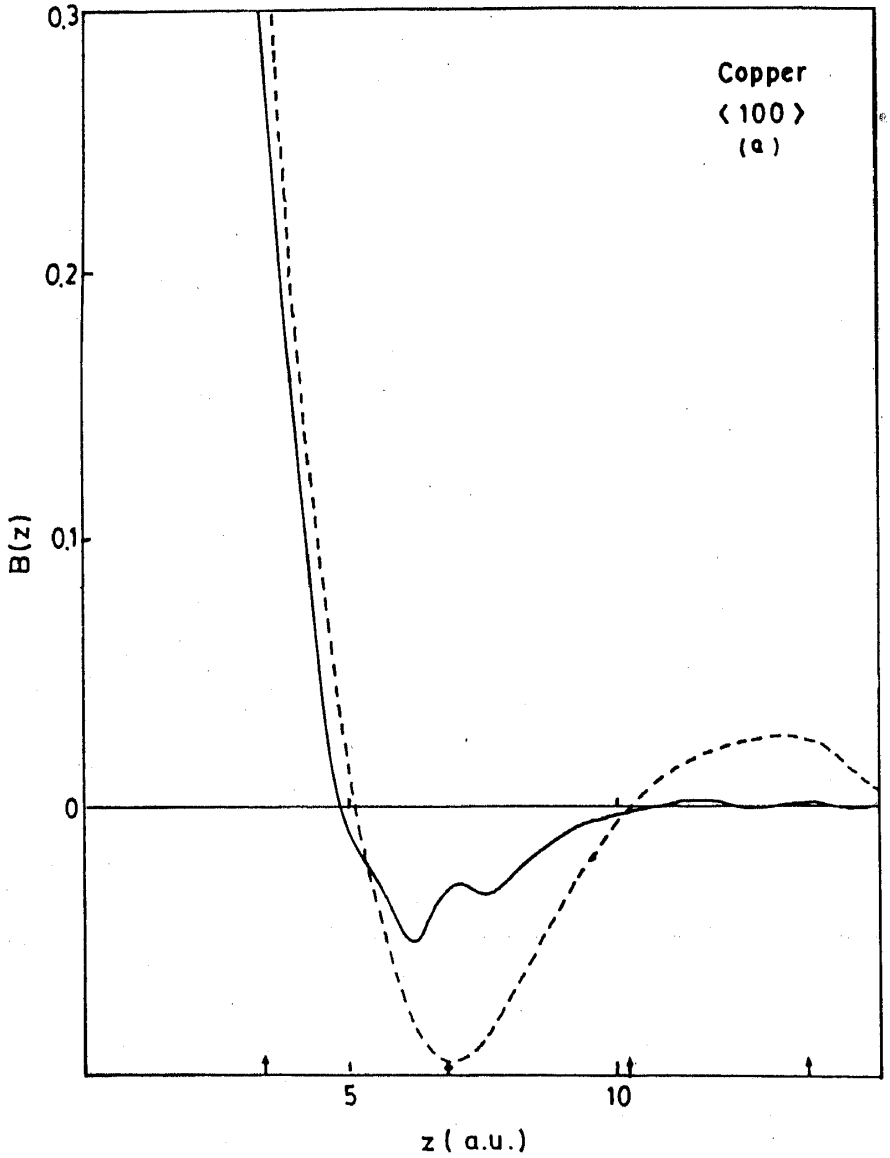

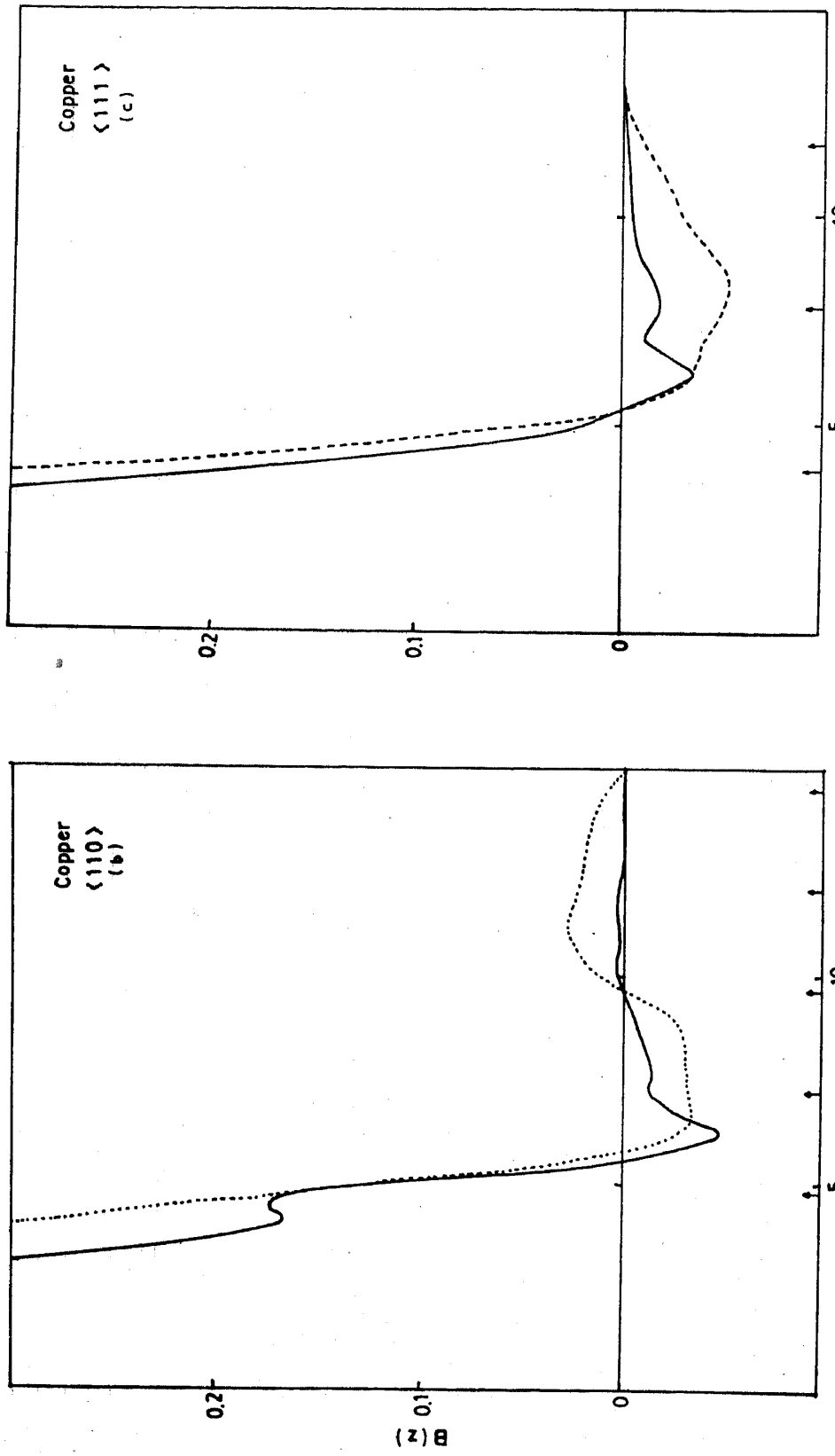

Figure 6. $B^{CP}(z)$–continuous curve, $B^{2\gamma}(z)$–dashed curve, along the three symmetry directions (**a**) ⟨110⟩, (**b**) ⟨110⟩ and (**c**) ⟨111⟩. Both the functions include core contribution and are convoluted by the respective experimental resolution functions. The arrows indicate the positions of the lattice vectors.

Table 2. Distances of lattice vectors and their projections on each of the symmetry direction and the corresponding values of the B function. The directions of the projected lattice vector is also indicated.

	⟨100⟩ Direction		
distances (a.u.)	3·411 ⟨110⟩	6·822 ⟨100⟩	10·233 ⟨110⟩
B^{CP}	0·2913	−0·0284	0·0008
$B^{2\gamma}$	0·3701	−0·0951	−0·0006
	⟨110⟩ Direction		
distances (a.u.)	2·416 ⟨011⟩	4·832 ⟨110⟩	7·248 ⟨011⟩	9·664 ⟨110⟩
B^{CP}	0·5115	0·1415	0·0128	0·0019
$B^{2\gamma}$	0·7771	0·1394	−0·0337	−0·0014
	⟨111⟩ Direction		
distances (a.u.)	3·9306 ⟨110⟩	7·8612 ⟨110⟩	11·7918 ⟨111⟩
B^{CP}	0·1725	0·0183	−0·00131
$B^{2\gamma}$	0·2524	−0·0524	−0·0107

Table 3. Zero crossings of the reciprocal form factors alongwith free electron values (distances are in a.u.).

	First crossing		Second crossing	
	⟨100⟩	⟨110⟩	⟨100⟩	⟨100⟩
Free electron	5·73	6·66	9·86	11·45
B^{CP}	4·85	5·50	10·48	9·54
$B^{2\gamma}(z)$	5·15	5·73	10·28	9·69

(Bauer and Schneider 1985) value of 0·112 + 0·007. A comparison of ⟨110⟩ direction for B^{CP} and $B^{2\gamma}$ shows additional hump around 4·5 a.u. for CP case. This is attributed to the overlap of d-lobes along that direction. As the positron preferentially senses the delocalized conduction electrons, and since the d-bands are well below the FS and are almost atomic like, such an hump is absent in $B^{2\gamma}$. This also causes $B^{2\gamma}$ to have appreciable value at large z as compared to B^{CP}. Table 3 gives zero crossings for the reciprocal form factors alongwith the free electron values. It is found that, $B^{2\gamma}$ values are nearer to the corresponding B^{CP} zero crossings, but the nature of the curve is close to the free electron-like behaviour.

4. Summary

We have reported the calculation of EMD and TPMD in copper using the self-consistent LCGO method within a single theoretical framework. The present study is the first to report the positron annihilation characteristics using LCGO method. The results for TPMD have been presented by taking its sections by the symmetry planes. Such 3D plots yield information about the nature of the FS. Comparison of the angular momentum decomposition of the EMD and the TPMD substantiates the fact that the positron preferentially annihilates with free *sp*-electrons rather than with the localized *d*-electrons. The 2D ACPAR surfaces and their cross-sections compare well with the experimental ones and also provide rich information about the FS topologies. This is greatly supported by the LCW folding procedure. The theoretical LCW-folded 2D ACPAR contours also compare well with the experimental ones and with the calculation by the APW method. The discrepancies that appear in these comparisons are attributed to the electron-positron correlation effects. The present results obtained within IPA would be useful in quantifying these effects with the help of experimental data.

Acknowledgements

We are thankful to Prof. R M Singru for illuminating discussions and Dr. Anjali Kshirsagar for critical examination of the manuscript. We are thankful to National Informatics Centre, Pune and Bhabha Atomic Research Centre, Bombay for computational facilities. Financial support from the Department of Science and Technology and Department of Atomic Energy, India, is thankfully acknowledged.

References

Bagayoko D, Laurent D G, Singhal S P and Callaway J 1980 *Phys. Lett.* **A76** 187
Bauer G E W and Schneider J R 1983 *Z. Phys.* **B54** 17
Bauer G E W and Schneider J R 1984a *J. Phys. Chem. Solids* **45** 675
Bauer G E W and Schneider J R 1984b *Phys. Rev. Lett.* **52** 2061
Bauer G E W and Schneider J R 1985 *Phys. Rev.* **B31** 681
Berko S 1979 *Positron Annihilation* (eds) R R Hasiguti and K Fujiwara (Sendai: Japanese Inst Metals) p. 65
Berko S 1983 *Positron Solid State Physics* (eds) W Brandt and A Dupasquier (Amsterdam: North-Holland) p. 64
Berko S and Mader J J 1975 *Appl. Phys.* **5** 287
Berko S, Haghgooie M and Mader J J 1977 *Phys. Lett.* **A63** 335
Brandt W and Dupasquier A 1983 *Positron Solid State Physics* (Amsterdam: North-Holland)
Bross H 1982 *J. Phys. F: Met. Phys.* **12** 2249
Bross H and Stohr H 1974 *Appl. Phys.* **3** 307
Cooper M J 1985 *Rep. Prog. Phys.* **48** 415
Cushner S, Erskine J C and Berko S 1970 *Phys. Rev.* **B1** 2852
Genoud P, Singh A K, Manuel A A, Jarlborg T, Walker E, Peter M and Weller M 1988 *J. Phys. F* **18** 1933
Haghgooie M, Mader J J and Berko S 1978 *Phys. Lett.* **A69** 293
Kahana S 1963 *Phys. Rev.* **129** 1622
Kaiser J H, West R N and Shiotani N 1986 *J. Phys. F* **16** 307
Kaiser J H, Walters P A, Bull C R, West R N and Shiotani N 1987 *J. Phys. F* **17** 1243
Kanhere D G and Singru R M 1977 *J. Phys. F* **7** 2603

Lock D G, Crisp V H C and West R N 1973 *J. Phys. F* **3** 561
Lock D G and West R N 1975 *Appl. Phys.* **6** 249
Loucks T L 1966 *Phys. Rev.* **144** 504
Manuel A A 1983 *Positron Solid State Physics* (eds) W Brandt and A Dupasquier (Amsterdam: North-Holland) p. 581
Matsumoto M and Wakoh S 1987 *J. Phys. Soc. Jpn* **56** 3566
Matsumoto M and Wakoh S 1988 *Physica* **B149** 57
Mijnarends P E 1973 *Physics* **63** 237
Mijnarends P E 1979 *Positrons in Solids* (ed.) P Hautojarvi (Berlin: Springer-verlag) p. 25
Mijnarends P E 1983 *Positron Solids State Physics* (eds) W Brandt and A Dupasquier (Amsterdam: North-Holland) p. 146
Mijnarends P E and Singru R M 1979 *Phys. Rev.* **B19** 6038
Pattison P, Hansen N K and Schneider J R 1982 *Z. Phys.* **B46** 285
Pattison P and Williams B 1976 *Solid State Commun.* **20** 585
Rabou L and Mijnarends P E 1984 *Solid State Commun.* **52** 933
Rajagopal A K, Singhal S P and Kimball J in Rajagopal A K 1980 *Adv. Chem. Phys.* **41** 59
Rath J, Wang C S, Tawil R A and Callaway J 1973 *Phys. Rev.* **B8** 5139
Rollason A J, Schneider J R, Laundy D S, Holt R S and Cooper M J 1987 *J. Phys. F* **17** 1105
Schulke W 1977 *Phys. Status Solidi* **B82** 229
Singh A K and Singru R M 1982 *J. Phys. F* **12** 685
Singh A K and Singru R M 1983 *J. Phys. F* **13** 2189
Singh A K and Singru R M 1984 *J. Phys. F* **14** 1751
Singh A K and Jarlborg T 1985 *J. Phys. F* **15** 727
Singh A K, Manuel A A, Jarlborg T, Mathys Y, Walker E and Peter M 1986 *Helv. Phys. Acta* **59** 410
Singh A K, Manuel A A, Singru R M and Peter M 1985 *Helv. Phys. Acta* **58** 640
Sundararajan V, Asokamani R and Kanhere D G 1988 *Phys. Rev.* **B38** 12653
Sundararajan V, Kanhere D G and Callaway J 1988 *Phys. Lett.* **A133** 521
Wakoh S, Berko S, Haghgooie M and Mader J J 1979 *J. Phys. F* **19** L231
Wang C S and Callaway J 1978 *Comput. Phys. Commun.* **14** 327
West R N, Mayers J and Walters P A 1981 *J. Phys.* **E14** 478
Williams B 1977 *Compton Scattering* (London: McGraw-Hill)